Extreme Mechanics Letters 49 (2021) 101491

Contents lists available at ScienceDirect

Extreme Mechanics Letters

journal homepage: www.elsevier.com/locate/eml

Dynamics of elastic hyperbolic lattices

Massimo Ruzzene [a,*], Emil Prodan [b], Camelia Prodan [c]

[a] P. M. Rady Department of Mechanical Engineering, University of Colorado Boulder, Boulder, CO, USA
[b] Department of Physics, Yeshiva University, New York, NY, USA
[c] Department of Physics, New Jersey Institute of Technology, Newark, NJ, USA

ARTICLE INFO

Article history:
Received 17 June 2021
Received in revised form 27 August 2021
Accepted 17 September 2021
Available online 8 October 2021

Keywords:
Hyperbolic lattices
Spectral properties
Mode localization

ABSTRACT

The hyperbolic space affords an infinite number of regular tessellations, as opposed to the Euclidean space. Thus, the hyperbolic space significantly extends the design space lattices, potentially providing access to unexplored wave phenomena. Here we investigate the dynamic behavior of hyperbolic tessellations governed by interactions whose strengths depend upon the distances between neighboring nodes. We find eigen-modes that are primarily localized either at the center or towards the boundary of the Poincaré disk, where hyperbolic lattices are represented. Hyperbolic translations of the seeding polygon produce distorted lattices, leading to a redistribution of the eigen-modes akin to edge-to-edge transitions. The spectral flow associated with these deformed lattices reveals a rich behavior that is characterized by modes that are spatially asymmetric and localized. The strength of the localization can be predicted from the slopes of the corresponding spectral branches, suggesting a potential topological origin for the observed phenomena. The rich yet predictable spectral flow and the high modal density of these lattices, along with the propensity of their modes to be strongly localized, suggest potential applications of hyperbolic lattices as vibration sensors, which operate over a large range of frequencies and exploit the sensitivity of localized modes to perturbations. In addition, hyperbolic lattices can inform the design of architected structural components with strong vibration attenuation and isolation capabilities.

1. Introduction

Significant attention has been recently devoted to hyperbolic lattices for applications related to mathematics, computer science and most recently, photonics [1–3]. These lattices tessellate the hyperbolic space, which in contrast to the Euclidean space, affords the opportunity for an infinite number of regular tessellations. Thus, hyperbolic lattices significantly extend the design space typically associated with lattices in Euclidean space, which are restricted to 2, 3, 6-fold symmetries as stipulated by the crystallographic restriction theorem [4]. Regular hyperbolic tessellations are obtained through a series of reflections and translations in hyperbolic space which lead to structures whose hierarchical patterns may be reflected in their physical properties and overall performance. The exploration of such properties and performance as it relates primarily to dynamics and vibrations is one of the goals of this study.

Recent investigations have employed hyperbolic lattice geometries for the demonstration of the existence of spectrally-isolated degenerate flat bands and unusual density of states for circuit quantum electrodynamics [1,2]. Also, topological phenomena in hyperbolic geometry for lattices under a uniform, pseudospin-dependent magnetic field, were shown to realize a non-Euclidean analog of the quantum spin Hall effect [3], and to display novel manifestations of the bulk-boundary correspondence principle [5]. A distinctive feature of these prior studies is that the interactions do not depend upon the distance of neighboring sites. In mechanics, such distance is of primary importance as it is intrinsically tied to the interaction strength. This key difference makes the study of hyperbolic lattices governed by mechanical interactions both novel and distinct relative to prior studies in terms of fundamental properties and potential relevance to applications. These applications include, for example, sensors, lightweight large structures, RF systems, and phase-array reflectors, all of which heavily rely on sensitivity to structural changes, on structural stability and on the ability to isolate and confine vibrations.

The objective of this paper is to conduct a preliminary investigation of the dynamic properties of hyperbolic lattice configurations. The interest lies on the broad variety of tessellations that are associated with hyperbolic geometries, by their inherent hierarchical configurations, and by their natural development onto curved surfaces. The study of hyperbolic lattices in mechanics is

* Corresponding author.
E-mail address: massimo.ruzzene@colorado.edu (M. Ruzzene).

https://doi.org/10.1016/j.eml.2021.101491
2352-4316/

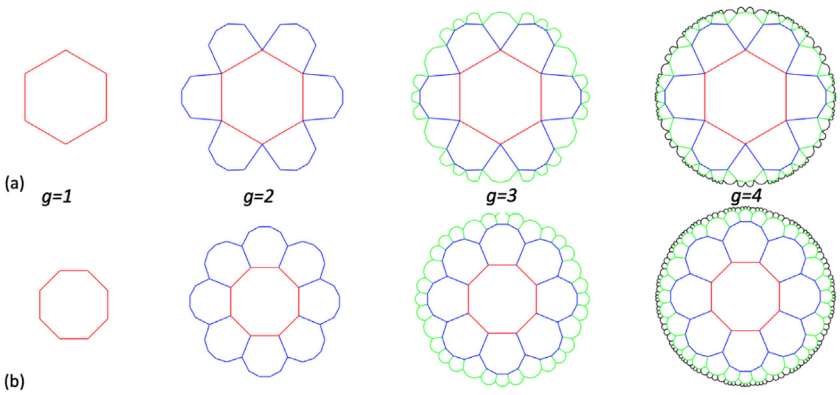

Fig. 1. Hyperbolic lattices corresponding to successive generations g: (a) lattices corresponding to Schläfli symbol $\{6, 4\}$, and (b) $\{8, 3\}$ lattice (b).

at its infancy, and as such it is rich in open questions as well as in opportunities for technological applications.

The paper is organized in 5 sections, including this introduction. Section 2 describes the geometry and the dynamic models employed, while Section 3 illustrates the spectral properties and the localized characteristics of most of the eigen-states (modes) that are found in regular hyperbolic lattices. Next, Section 4 investigates these properties and their sensitivity to variations resulting from hyperbolic translations of the originating polygon. Finally, Section 5 summarizes the main findings of the work.

2. Hyperbolic lattices: Geometry and dynamic model

We focus on the dynamic behavior of two-dimensional (2D) hyperbolic lattices, here represented in the Poincaré disk defining the projection of a hyperboloid onto the unit disk [6,7]. The negative curvature of the hyperbolic plane differentiates hyperbolic lattices from their Euclidean counterpart [3]. For example, in the hyperbolic plane, the sum of internal angles of a polygon is smaller than in its Euclidean counterpart, which allows denser contact of polygons at vertices. For example, while only four squares can be contacted in an Euclidean square lattice, any number of squares $q > 4$ can be in contact in hyperbolic lattices.

The lattice degrees of freedom are expressed by the Schläfli symbol $\{p, q\}$, where the integers p and q respectively denote tessellations of q contacting p-sided regular polygons, with $q > 4$. Given a p-sided seed polygon, hyperbolic tilings are achieved by recursively adding neighboring polygons to the outermost edges, such that two polygons sharing an edge are connected by a hyperbolic reflection. The hyperbolic reflection of a point against a hyperbolic geodesic is analogous to the reflection of a point against a straight line in the Euclidean plane: both define the mirror symmetric copy of a point relative to a line. The analytic expression of the hyperbolic reflection can be found in [6] (see Chapters 7 for examples) and the interested readers may also visit the link in [8] for visualizations, examples and tutorials. With reference to Fig. 1, the tessellation process can be described as follows: Consider the seeding polygon, marked as generation $g = 1$ in Fig. 1. Then each point of the polygon is reflected about each of its sides. If the originating polygon is a hexagon, as for example in Fig. 1a, these reflections produces 6 polygons which are said to belong to the second generation of the lattice, (blue polygons in Fig. 1). Repeating the operation for each polygon from the second generation leads to the third generation (green polygons in Fig. 1). Progressing with the process recursively fills the Poincaré disk [6,9], as exemplified in Fig. 1 for two seeding polygons. The outcomes are tree-like geometries consisting of repeating units that define structures that are inherently hierarchical. Examples of such structures corresponding to various Schläfli symbols are illustrated in Fig. 2.

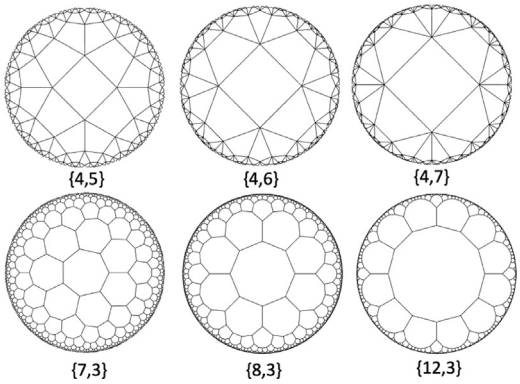

Fig. 2. Examples of hyperbolic lattices which sample a variety of Schläfli symbols $\{p, q\}$.

Based on these geometries, we design a discrete mechanical system by assigning a mass to each node of a hyperbolic lattice, with a specified degree of freedom, and connect the nearest neighbors by linear elastic links. We assume that the masses are identical and equal to $m = 1$, and move along the z direction perpendicular to the plane of the lattice. Henceforth, the system is described by the Lagrangian

$$\mathcal{L} = \tfrac{1}{2} m \sum_{\boldsymbol{n}} \dot{z}_{\boldsymbol{n}}^2 - \sum_{\boldsymbol{n},\boldsymbol{n}'} W(\boldsymbol{r}_{\boldsymbol{n}} - \boldsymbol{r}_{\boldsymbol{n}'}, z_{\boldsymbol{n}} - z_{\boldsymbol{n}'}). \tag{1}$$

where $\boldsymbol{r}_{\boldsymbol{n}}$ defines the location of the nth mass, and $z_{\boldsymbol{n}}$ is the corresponding out-of-plane motion. Also in Eq. (1), W is the interaction potential, which is defined as

$$W(\boldsymbol{r}, z) = \tfrac{k}{2} z^2 / |\boldsymbol{r}|, \tag{2}$$

where k is an interaction constant, which is here set equal to 1 for convenience. The potential in Eq. (2) describes interactions whose strength is inversely proportional to the Euclidean distance $|\boldsymbol{u}|$ between neighboring nodes. This is a distinctive difference with respect to prior work on circuit quantum electrodynamics [1,2] and on non-Euclidean analogs of the quantum spin Hall effect [3], where interactions are independent upon the distance of neighboring sites. Assuming a mechanical realization of this lattice, such distance becomes of primary importance as it is intrinsically tied to the stiffness of a ligament. This distinctive feature makes the study of hyperbolically inspired lattices governed by mechanical interactions rich in open questions related to the effect of tessellations and of lattice distortions as investigated in the upcoming sections.

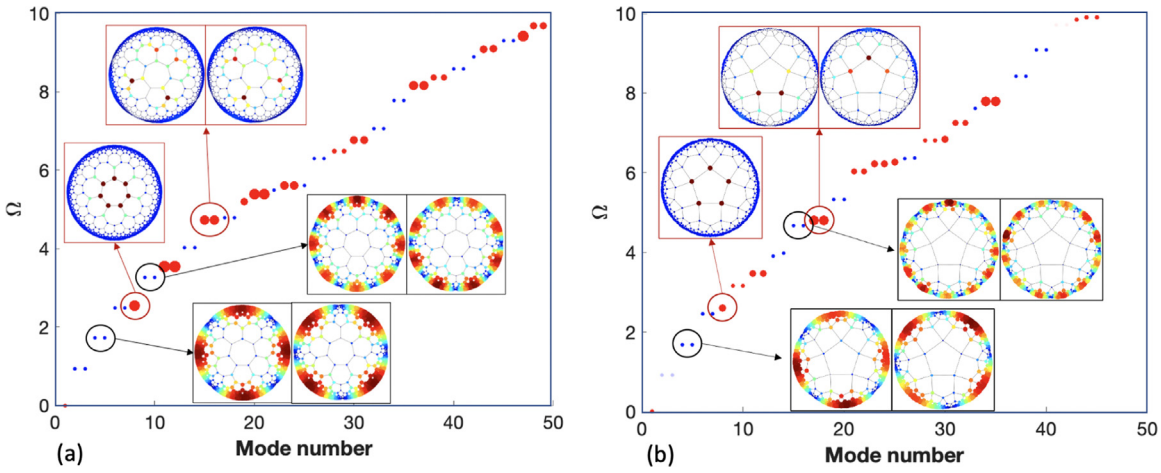

Fig. 3. Vibrational spectrum for the $\{7, 3\}$ (a), and $\{5, 4\}$ (b) lattices, with eigen-modes displaying distinct bulk (red) or boundary (blue) spatial profiles. Selected eigenstates show the presence of degenerate eigenfrequency pairs associated with eigenstates that are rotated copies of each other, in conjunction with modes that are mostly localized at the center of the disk. (For interpretation of the references to color in this figure legend, the reader is referred to the web version of this article.)

3. Spectral analysis and mode localization

We first investigate the spectral characteristics of various (finite) hyperbolic tessellations nucleated from the center of the hyperbolic disk. All lattices investigated in this study are of generation $g = 6$ which is found sufficient in terms of frequency range of the dynamic behavior and degree of hierarchy. The cases for $\{7, 3\}$ and $\{4, 5\}$ lattices are chosen here for illustration purposes, and similar results can be found for other tessellations. The distribution of the first 40 natural eigenvalues Ω versus the mode number are shown in Fig. 3.

In the plots, each eigen-frequency is represented by a solid circle whose color (red or blue) and size are defined by a localization index $\mathcal{I}^{(n)}$, which, for the nth eigenvector $\boldsymbol{\Phi}^{(n)}$, is defined as:

$$\mathcal{I}^{(n)} = \frac{\sum_{i\in\mathcal{C}} \Phi_i^{(n)}}{\sum_i^N \Phi_i^{(n)}}. \tag{3}$$

Here, $\Phi_i^{(n)}$ is the amplitude of the nth mode at lattice site i, N denotes the total number of nodes in the lattice, while $\mathcal{C}$ identifies the subset of such nodes that belong to the first and second generation. Thus, $\mathcal{I}^{(n)} \to 1$ identifies an eigenmode that is fully localized in the center of the crystal, while $\mathcal{I}^{(n)} \to 0$ corresponds to modes that are mainly localized towards to the edges of the crystal. The blue/red colors correspond to $\mathcal{I}^{(n)} < 0.5$ and $\mathcal{I}^{(n)} > 0.5$, respectively, hence they separate the modes into two classes with either edge or center localized character. A finer account of the localization character is supplied by the sizes of the markers which are proportional to $\mathcal{I}^{(n)}$, hence a larger circle describes a higher degree of center-localization. This mode analysis can and will be applied also to the crystals nucleated from points other than the center of the Poincaré disk (Section 4).

Fig. 3 shows that the modes mostly appear in pairs, but not all the time. This phenomenon is specific to the lattices nucleated from the center of the Poincaré disk and is related to the rotational symmetry of the lattice, and, more precisely, with the fact that the representation sectors of the cyclic C_p group with conjugate characters are mapped into each other by the complex conjugation. Hence, the spectral degeneracies correspond to pairs of modes from such conjugate sectors, which appear to be simply rotated versions of each other. The non-degenerate modes correspond to the representation sector with trivial character, which is self-conjugate. Examples of such modes are shown in Fig. 3 (see modes in the dark-framed inserts). As one can see, the blue resonances mostly occur in pairs. However, the second group of modes, characterized by $\mathcal{I}^{(n)} \to 1$ and corresponding to strong localization towards the center of the lattice, alternate between degenerate and non-degenerate modes and display different levels of spatial symmetry (see the modes in the red-framed inserts).

As it is always the case with lattice systems, spatial variations increase the energy of a vibrational mode, hence the low energy modes tend to be highly de-localized. Our hyperbolic crystal, however, becomes stiffer closer to the boundaries, hence the modes not localized near the center will feel an environment that promotes higher energies. As such, the spectral data seen in Fig. 3 is a result of a synergy between the spatial variation and the spatial location of the modes. As a result, eigen-modes that are centrally localized and modes de-localized along the boundary coexist at comparable energies, a scenario that is completely absent in uniform Euclidean lattices. This leads to an interesting mechanical response to the deformations of the lattice, which is explored in the next section.

4. Distorted hyperbolic lattices

A hyperbolic tessellation can be nucleated from any point of the Poincaré disk by simply translating the seed polygon. From the pure hyperbolic geometry point of view, all such translated tessellations are completely equivalent. However, we recall that, in mechanical lattices, the interactions between masses at the nodes (see Eq. (2)) are inversely proportional to the Euclidean distances between the positions, hence our hyperbolic tessellations should be treated as point-patterns in the Euclidean space. Hyperbolic displacements of the seeding polygon in certain directions lead to cyclic distortions of the crystal, as it is illustrated in Fig. 4 for the $\{4, 5\}$ (a) and the $\{7, 3\}$ (b) lattices. Indeed, when $r = \pm 2$ in this figure, the hyperbolically translated seed polygon (shaded gray in the figure) becomes identical to a polygon from the original lattice, hence the tessellation algorithm produces identical infinite lattices. These distortions can be also interpreted in light of a projection operation from a point in space, which is consistent with the Poincaré disk representation of these lattices. In this context, the distorted configurations correspond to stereoscopic projections of the same lattice from a point that translates in space [6].

In this work, we focus on finite lattices (6 generations), which break the repetitive character of the deformation process. The

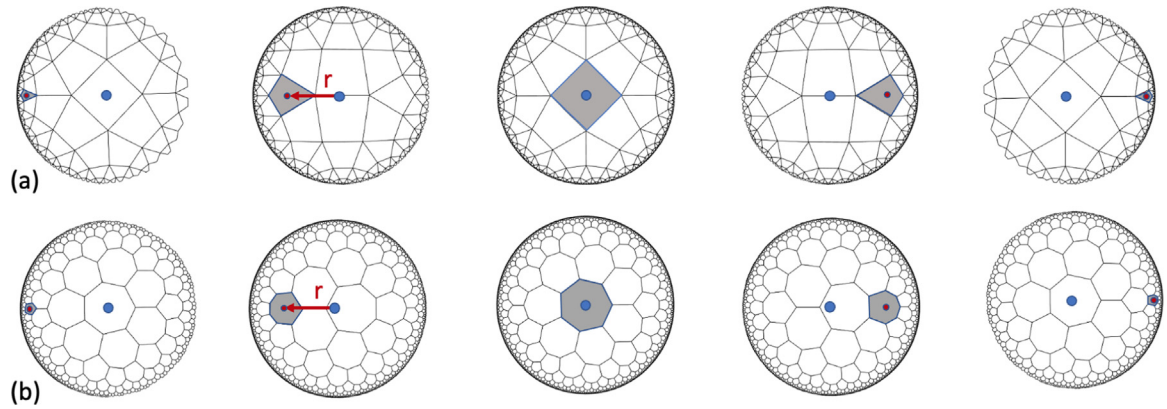

Fig. 4. Distorted {4, 5} and {7, 3} lattices ((a) and (b) respectively) are obtained from the horizontal translation of the originating polygon. Such translation r leads to a repeating pattern in the event of a hyperbolic tessellation encompassing infinite generations. The process can be also considered as the result of the stereoscopic projection of the lattice from a varying point in space [6].

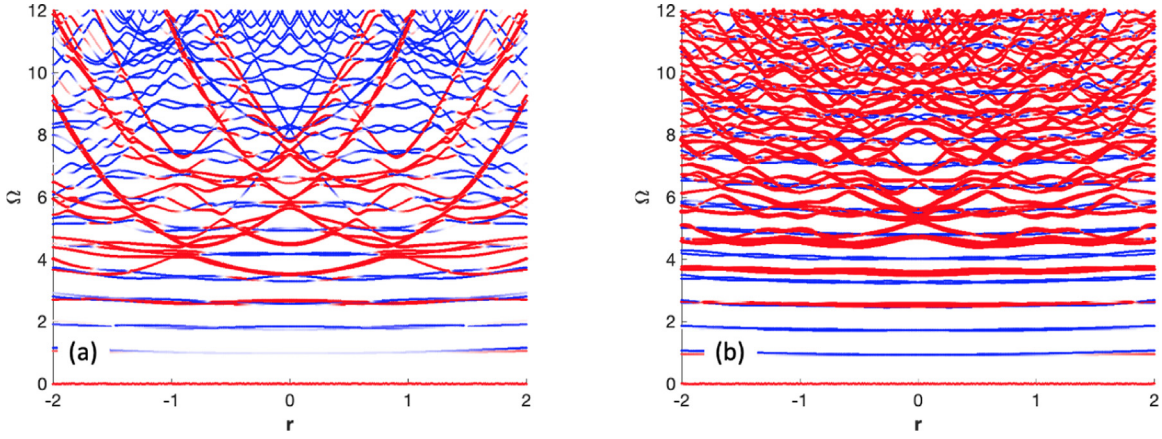

Fig. 5. Spectral properties of distorted {4, 5} and {7, 3} lattices ((a) and (b) respectively).

spectral flow induced by the distortions are shown in Fig. 5. Complex emerging patterns for the spectral branches illustrate an extremely rich dynamic behavior. The modes localized in the center of the crystal, *i.e.* those with significant amplitudes inside the first and second generation of lattice points around the seed polygons, shown in Fig. 4, have been identified with the protocols described in the previous section, and color coded based on the localization index $\mathcal{I}^{(n)}$ of Eq. (3). Remarkably, the spectral flow associated to these modes assembles in distinct continuous curves in Fig. 5(a) (see the red highlights). These spectral curves can be understood from the re-scaling of the local bond lengths around the seed polygon as $2/(1-d_r^2)$, where d_r is the Euclidean distance from the center of seed polygon to the center of the disk. Indeed, as the seed polygon is displaced away from the center of the disk, the modes localized around it experience a lattice with shorter bonds and, as such, the frequencies of the center-localized modes are expected to scale as $\sqrt{2/(1-d_r^2)}$ with parameter r. This is the equation governing the red curves clearly seen in Fig. 5(a). The spectral flow of the center-localized modes in Fig. 5(b) is more complicated because the set C in Eq. (3) contains many more points, hence in Fig. 5(b) we see a much larger number of localized modes.

As we mentioned in the previous section, center and edge localized modes coexist in the same window of frequencies, and this leads to interesting synergy between the spectral flows of the center and edge localized modes. Indeed, upon increasing the parameter r, a center-localized mode moves up in frequency, but the edge localized modes are less affected and they hover around a fixed frequency. When an edge (blue) band meets a red parabola, a hybridization happen and the blue bands appear to peal off and then merge into the red bands, via sharp veering points [10]. In addition, various values of r correspond to the coalescence of multiple frequencies, which is a potential indication of the occurrence of spectral singularities, which may be associated with exceptional points, here induced by distortions, as opposed to parity-symmetry time conditions [11,12]. Such singularities and their sensitivity to perturbations are potentially of great interest for sensing purposes, and specifically in relation to their sensitivity to lattice perturbations. These activities may be inspired by the recent strong interest on exceptional points for novel sensing configurations [13]. Furthermore, modal crossings and associated hybridization may also be highly relevant for the purpose of exploiting vibrations for information transfer, as the ability for a mode to transition from being edge localized, to being more distributed, and to eventually become localized in the center portion of the lattice could form the basis for efficient transfer of signals across the lattice with minimal changes in frequency.

A selection of eigen-modes for the {4, 5} lattice are presented in Fig. 6, to confirm how the color coding adopted provides a good indication of the localization of the modes. This is illustrated for example for the modes denoted with (1) in the figure, which corresponds to a boundary localized mode, which is distributed across the entire edge. This mode occurs on a branch that is generally flat, and therefore not significantly affected by the variation of the translation parameter r. A similar observation

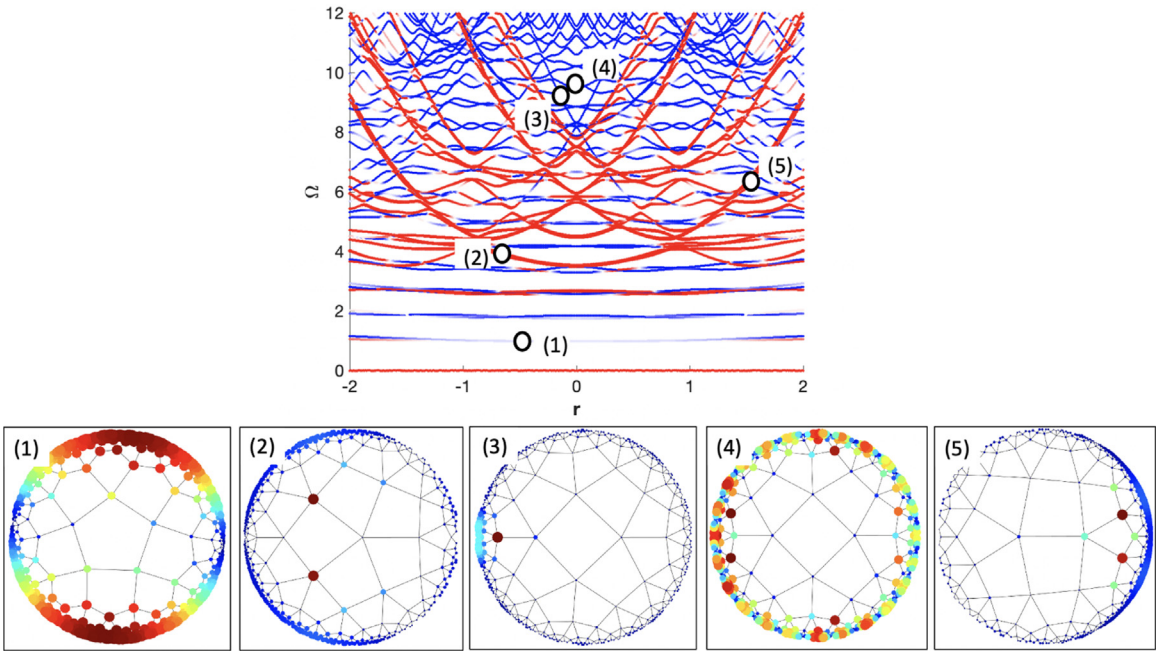

Fig. 6. Distorted $\{4, 5\}$: selection of eigenmodes associated with flat branches (modes (1) and (4)) are characterized by edge-localized modes that are not strongly affected by the variation of r. These modes are characterized by a high degree of rotational symmetry. In contrast, modes corresponding to branches of higher slopes appear to be localized and non-symmetric (modes (2,3) and (5)). The circumferential location of the localization is related to the slope of the branch: left-localized for modes belonging to a branch of negative slope (modes (2,3)) and right-localized for a positive branch (mode (5)).

can be made for mode (4), which occurs at higher frequencies and it is associated with a branch of moderate slope. In contrast, modes (2,3,5) are localized along the circumferential direction, *i.e.* they are not uniformly distributed along the angular coordinate, and are respectively localized at the center (2), and along the edge (3,5). Modes (3,5) in particular are highlighted out of branches that are highly sensitive with respect to r, and as a result are strongly asymmetric. Notably, the slope of the branch is correlated to the degree of localization along the circumferential direction: the steeper the branch, the stronger the circumferential localization and the related asymmetry (modes (2,3) and (5)). The circumferential location of the localization is also related to sign of the slope of the branch: left-localized for modes belonging to a branch of negative slope (modes (2,3)) and right-localized for modes along a positive slope branch (mode (5)). This suggests the possibility of predicting the spatial characteristics of localized modes through topological considerations that may be applied to the spectral branches.

A final set of results illustrate the effects of a sweep of the parameter r on a specific mode, which is illustrated in Fig. 7. In this context, the parameter r is considered as an adiabatic parameter that is reminiscent of the dynamics of a phason in non-commensurate lattices [14–16]. The range of variation of the mode is highlighted by the black rectangular box in Fig. 7. Spanning of r in the highlighted range shows how a mode initially localized at the inner portion is made to move and evolve through a process that is reminiscent of a topological pump [16]. The mode at the initial considered value of $r = -0.2$ is shown in the top left corner of Fig. 7. As r is varied, the mode shifts in an apparent counterclockwise motion, which can be followed by looking at the sequence of mode shapes presented in a counterclockwise arrangement in Fig. 7. At $r = 0$, the mode loses localization and appears symmetric, while as r grows and becomes positive, the mode regains its localized nature, at a location that is symmetric with respect to the negative values of r. These results show that a simple translation of the originating polygon leads to a predictable re-location of the localized modes, a phenomenon that is quite analogous to what has been already observed in periodically modulated lattices in Euclidean space. Indeed, it has been observed [15–17] that spatial modulations of lattice properties and/or geometry can lead to mode localization, at locations that are entirely controlled by the phase of such periodic material/geometrical modulations. This dynamical characteristic was used to drive an edge-to-edge transition of an eigen-mode, hence to controllably transfer energy or information across a mechanical structure, by simply modifying the phase of the modulation [14,16]. Here, the translation of the originating polygon produces the same effect, as it induces periodic variations of the lattice geometry that are accompanied by spatial re-locations of the localized modes. While these similarities are of considerable interest for the fundamental understanding of the dynamics of periodic lattices, both euclidean and hyperbolic, our observations may have interesting practical implications. Indeed, for a hyperbolic crystal with Schläfli symbol $\{p, q\}$, we can use the symmetry and translate along p independent directions to generate the same effects. This supplies a knob to control the location of the localize modes practically throughout the mechanical structure. Hyperbolic lattices in the Poincaré disk may be mapped to different shapes and can form the basis for novel structural components that are hierarchical in nature, and that are characterized by a dynamic behavior that is rich in modes that are strongly localized in space. These structural components could lead to novel designs of lattice structures of a variety of tessellations that have significant vibration isolation characteristics, along with possibly novel mechanical properties owing to their hierarchical structure.

5. Conclusions

The dynamic properties of elastic hyperbolic lattices are investigated to highlight their spectral characteristics. These include eigenvectors that are localized at the center alternating with ones that are localized at the boundary of the Poincaré disk. The spectral branches also reveal repeated eigenvalues that suggest

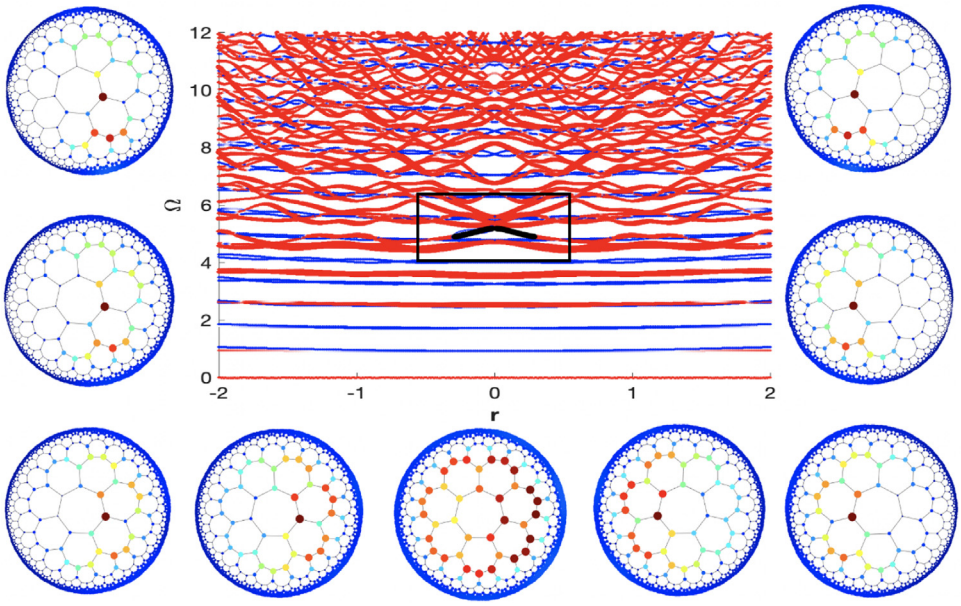

Fig. 7. Distorted {7, 3} lattice spectra, and variation of eigen-modes along a selected branch (bold line in square frame): the localization of the mode evolves along a circumferential directory as r varies, leading to a process which is reminiscent of a topological pump [16].

spectral degeneracies resulting from the rotational symmetry of the lattices. Next, distortions are introduced as hyperbolic translations of the generating polygon. These cause shifts of the eigenvalues which trace spectral branches forming complex spectral patterns. The slope of the branches are indicative of the strength of modal localization, which is quantified in terms of a localization parameter. Following of specific branches illustrates of the possibility of controlling a transition of the area of deformation which is driven by lattice distortions. The complex spectral characteristics of hyperbolic lattices suggest a number of applications related to lattices capable of localizing vibrations, that are highly sensitive to perturbations, and that are defined by hierarchical structures that can be developed on curved surfaces.

Declaration of competing interest

The authors declare that they have no known competing financial interests or personal relationships that could have appeared to influence the work reported in this paper.

Acknowledgments

M. Ruzzene gratefully acknowledge the support from the National Science Foundation (NSF), USA through the EFRI1741685 grant and from the Army Research Office, USA through grant W911NF-18-1-0036. E. Prodan and C. Prodan acknowledge support from the W. M. Keck Foundation, USA. E. Prodan acknowledges additional support from National Science Foundation, USA through the grant DMR-1823800.

References

[1] A.J. Kollár, M. Fitzpatrick, A.A. Houck, Hyperbolic lattices in circuit quantum electrodynamics, Nature 571 (7763) (2019) 45–50.
[2] A.J. Kollár, M. Fitzpatrick, P. Sarnak, A.A. Houck, Line-graph lattices: Euclidean and non-euclidean flat bands, and implementations in circuit quantum electrodynamics, Comm. Math. Phys. 376 (2020) 1909–1956.
[3] S. Yu, X. Piao, N. Park, Topological hyperbolic lattices, 2020, Phys. Rev. Lett. 125, 053901.
[4] S. Elliott, The Physics and Chemistry of Solids, Wiley, 1998.
[5] V. Mathai, G.C. Thiang, Topological phases on the hyperbolic plane: fractional bulk-boundary correspondence, Adv. Theor. Math. Phys. 23 (2019) 803–840.
[6] J.G. Ratcliffe, S. Axler, K. Ribet, Foundations of Hyperbolic Manifolds, vol. 149, Springer, 2006.
[7] S. Katok, Fuchsian Groups, University of Chicago Press, 1992.
[8] Interactive hyperbolic tiling in the poincaré disc.
[9] M. von Gagern, J. Richter-Gebert, Hyperbolization of Euclidean ornaments, Electron. J. Combin. 16 (2) (2009) R12.
[10] C. Pierre, Mode localization and eigenvalue loci veering phenomena in disordered structures, J. Sound Vib. 126 (3) (1988) 485–502.
[11] W. Chen, Ş.K. Özdemir, G. Zhao, J. Wiersig, L. Yang, Exceptional points enhance sensing in an optical microcavity, Nature 548 (7666) (2017) 192–196.
[12] M.-A. Miri, A. Alu, Exceptional points in optics and photonics, Science 363 (6422) (2019).
[13] M.I. Rosa, M. Mazzotti, M. Ruzzene, Exceptional points and enhanced sensitivity in PT-symmetric continuous elastic media, J. Mech. Phys. Solids (2021) 104325.
[14] W. Cheng, E. Prodan, C. Prodan, Experimental demonstration of dynamic topological pumping across incommensurate acoustic meta-crystals, Phys. Rev. Lett. 125 (2020) 224301.
[15] X. Ni, K. Chen, M. Weiner, D.J. Apigo, C. Prodan, A. Alù, E. Prodan, A.B. Khanikaev, Observation of hofstadter butterfly and topological edge states in reconfigurable quasi-periodic acoustic crystals, Commun. Phys. 2 (1) (2019) 1–7.
[16] M.I. Rosa, R.K. Pal, J.R. Arruda, M. Ruzzene, Edge states and topological pumping in spatially modulated elastic lattices, Phys. Rev. Lett. 123 (3) (2019) 034301.
[17] R.K. Pal, M.I. Rosa, M. Ruzzene, Topological bands and localized vibration modes in quasiperiodic beams, New J. Phys. 21 (9) (2019) 093017.